CLM-P817

Tearing modes in toroidal geometry

J.W. Connor, S.C. Cowley, R.J. Hastie, T.C. Hender,

A. Hood* and T.J. Martin

Culham Laboratory, Abingdon, Oxfordshire OX14 3DB, UK

(EURATOM/UKAEA Fusion Association)

Abstract

The separation of the cylindrical tearing mode stability problem into a resistive resonant layer calculation and an external marginal ideal mhd (Δ') calculation is generalised to axisymmetric toroidal geometry. The general structure of this separation is analysed and the marginal ideal mhd information (the toroidal generalisation of Δ') required to discuss stability is isolated. This can then, in principle, be combined with relevant resonant layer calculations to determine tearing mode growth rates in realistic situations. Two examples are given: the first is an analytic treatment of toroidally coupled ($m = 1$, $n = 1$) and ($m = 2$, $n = 1$) tearing modes in a large aspect ratio torus; the second, a numerical treatment of the toroidal coupling of three tearing modes through finite pressure effects in a large aspect ratio torus. In addition we discuss the use of a coupling integral approach to determining the stability of coupled tearing modes. Finally, the possibility of using initial value resistive mhd codes in realistic toroidal geometry to determine the necessary information from the ideal mhd marginal solution is discussed.

*St. Andrews University, St. Andrews, North Haugh, Fife, Scotland KY16 9SS

(Submitted for publication in Physics of Fluids).

Culham Laboratory
United Kingdom Atomic Energy Authority
Abingdon
Oxfordshire OX14 3DB

May 1987

I. Introduction

The stability of tearing modes in the cylindrical limit of a toroidal pinch can be determined directly by numerically solving the resistive mhd eigenvalue equations[1] or, in the limit of large Lundquist number (magnetic Reynold's number) S, by a semi-analytic asymptotic matching procedure.[2,3] In this latter approach one identifies a narrow layer of width $S^{-2/5}$ near the resonant surface $q(r) = m/n$, where m and n are the poloidal and toroidal mode numbers and q is the safety factor, in which resistivity plays an important role. Elsewhere marginally stable ideal mhd equations are appropriate. The growth rate γ of tearing modes follows from matching the ideal mhd solutions to the resistive layer solutions and takes the form

$$\Delta' = \Delta_R(\gamma) \tag{1}$$

Here $\Delta_R(\gamma)$ can be calculated analytically[2,3] from the resistive layer equations while Δ' is calculated numerically from the solution for the perturbed magnetic flux function ψ in the ideal region.[4] This perturbation satisfies the correct boundary conditions at the centre and edge of the plasma column but has a discontinuity Δ' in its logarithmic gradient across the resonant surface. Thus the entire role of the ideal solution is represented by a single quantity Δ'.

Furthermore the separation of the problem into a resonant layer calculation and a calculation of Δ' means that the resistive mhd physics used in calculating Δ_R can be replaced by more realistic models for high temperature plasma (involving diamagnetic effects,[5] collisionless and semi-collisional electron dynamics,[6] finite larmor radius effects,[6,7]

etc.) without changing the significance of Δ' in equation (1).

Whereas the cylindrical problem is clearly solved in principle, and largely in practice too, this is not the case in an axisymmetric torus where a single eigenmode contains a number of poloidal harmonics. Recent developments in initial value resistive mhd codes have allowed direct attacks on tearing mode stability of large[8,9] and tight[10,11] aspect ratio tokamaks at moderate values of $S \sim 10^6$. Extension to higher values of S makes great demands on computing resources and the prospects for treatment of more realistic plasma dynamics than resistive mhd appear to be limited. Thus a breakdown of the problem into separate treatments of resonant layers matched to ideal mhd solutions in between, as in the cylinder, would be desirable.

The main concern of this paper is the effect of toroidicity (and hence the presence of a number of poloidal harmonics) on the ideal solutions between resonant surfaces and the consequences for the nature of the matching problem at those resonant surfaces. However we note that toroidicity also affects the solution within the resonant layers, namely $\Delta_R(\gamma)$. Thus the stabilising influence of favourable average curvature on tearing modes has been examined analytically[12] (and even used to interpret the behaviour of initial value codes[11]). Similarly the effect of toroidally trapped particles on the dynamics near the resonant surface has been discussed.[13]

In Section II of this paper we describe the general structure of the axisymmetric toroidal problem involving a number of resonant surfaces, providing definitions of the quantities that replace the single object Δ' of the cylindrical case. (Appendix B gives a more detailed and precise discussion similar in terms to that used in the Resistive PEST Code.[14])

This information can then be associated with appropriate realistic descriptions of the physics at the resonant surfaces by imposing the relevant asymptotic matching conditions at these surfaces to determine the dispersion relation for toroidal tearing modes.

As a first application of the formulation we discuss in Section III the special case of the toroidal coupling of $(m = 1, n = 1)$ and $(m = 2, n = 1)$ tearing modes in a large aspect ratio tokamak. In this case it is possible to derive a completely analytic dispersion relation.[15]

In Section IV we derive the structure of the dispersion relation for toroidally coupled tearing modes with principal poloidal harmonics $m - 1$, m and $m + 1$ in a large aspect ratio tokamak and relate this to the coupling integral approach applied to the case of zero pressure gradient.[16]

The Resistive PEST code[14] is an ambitious example of the asymptotic matching approach and has been successfully used to examine the stability of tearing modes in arbitrary toroidal configurations at zero pressure. However some difficulty has been experienced in dealing with finite pressure since the ideal perturbations at the resonant surface then become more singular. In Section V we apply the dispersion relation of Section IV to a case involving finite pressure, namely a large aspect ratio tokamak in which the toroidal coupling arises through finite pressure gradient terms. In order to calculate the appropriate quantities from the ideal mhd solutions we use a shooting code with appropriate prescriptions for dealing with the singularities at the resonant surfaces caused by the pressure gradients. This contrasts with earlier calculations from which such effects are absent.[17] Choosing a simple

resistive mhd model for the resonant layer (this model excludes the Glasser effect) we examine the influence of finite pressure on stability.

In Section VI we discuss the possibility of using our general formalism in conjunction with a resistive mhd initial value code[10] to produce results for arbitrary resonant layer models in fully toroidal geometry. Finally we draw conclusions in Section VII.

II The Structure of the Toroidal Tearing Mode Eigenvalue Problem

In this Section we describe the structure of the toroidal tearing mode eigenvalue problem in axisymmetric toroidal geometry. For a tearing mode with toroidal mode number n there will, in general, be a number of so called resonant surfaces labelled by a radius r_m at which the safety factor $q(r_m) = m/n$, with m an integer. Between these resonant surfaces non-ideal effects are negligible and, because tearing modes evolve on a much longer timescale than Alfvenic, the plasma can be described by marginal ideal mhd equation for the perturbed poloidal flux ψ (see Appendix A). However, at a radius r_m the m^{th} poloidal harmonic of the toroidal tearing mode will be resonant and non-ideal and inertial effects become important in a narrow layer surrounding r_m. The solution of the appropriate non-ideal equations in this resonant layer must be matched to the ideal mhd equations on either side. In order to simplify the discussion we restrict ourselves in this Section to cases in which the ideal solutions behave as $\psi = C_0 + C_1(r-r_m)$ in the vicinity of r_m, where C_0 and C_1 are constants. This limits us to situations in which the Mercier indices[12] are zero and unity, but as shown in the more precise formulation of Appendix B, the present discussion exhibits the essential features of the general problem. With this caveat the matching

can be represented as a prescription for a discontinuity in the radial derivative of ψ_m across the resonant layer at r_m

$$\Delta'_m \equiv \lim_{\varepsilon \to 0} \left(\frac{\psi'}{\psi} \Big|_{r=r_m+\varepsilon} - \frac{\psi'}{\psi} \Big|_{r=r_m-\varepsilon} \right) = \Delta_m(\omega) \qquad (2)$$

where prime denotes a radial derivative and ω is the mode frequency. The quantity $\Delta_m(\omega)$ depends on the model for the dynamics in the resonant layer. Thus, for example, with a low pressure, resistive mhd model for the layer[12]

$$r\Delta_m(\omega) = \gamma^{5/4}\sqrt{2}\,\pi \frac{\Gamma(3/4)}{\Gamma(1/4)} \left(\frac{4\pi r^2}{\eta}\right)^{3/4} \left(\frac{\sqrt{4\pi\rho}}{m(dB_\theta/dr)}\right)^{1/2} \qquad (3)$$

where $\gamma = -i\omega$ is the growth rate, ρ the density and η the resistivity.

The procedure we adopt is to expand the perturbed flux function ψ of the toroidal tearing mode as a Fourier series of poloidal harmonics. These satisfy the ideal marginal equations between resonant surfaces but the m^{th} harmonic ψ_m suffers a discontinuity Δ'_m in its radial derivative at the resonant surface r_m if this lies in the plasma. As we shall see below, imposing appropriate boundary conditions on the set $\{\psi_m\}$ at the centre and boundary of the plasma column leads to a relation

$$f(\Delta'_{m_1}, \Delta'_{m_2} \ldots) = 0 \qquad (4)$$

between those Δ'_{m_i} where m_1, m_2, etc. are the harmonics which are

resonant within the plasma. Inserting a set of matching conditions

$$\Delta'_{m_i} = \Delta_{m_i}(\omega) \qquad i = 1, 2..... \tag{5}$$

into Eq.(4) yields an eigenvalue equation for ω. While this eigenvalue equation depends on the details of the particular layer models invoked in determining $\Delta_{m_i}(\omega)$ of Eq.(5), the fundamental relation (4) is generic, depending only on the marginal ideal mhd solutions - it is this relation we wish to emphasize in this paper.

In order to establish the nature of relation (4) we first consider a specific example in which the tearing mode is represented by three poloidal harmonics $m-1$, m and $m+1$, of which only m and $m+1$ possess rational surfaces within the plasma at r_m and r_{m+1} respectively. The generalisation to an arbitrary case is straight forward and is presented in Appendix B. The ideal marginal mhd equations for the quantities $\psi_{m-1}(r)$, $\psi_m(r)$ and $\psi_{m+1}(r)$ take the form of three coupled radial differential equations (see Appendix A) which can be represented schematically as

$$\begin{aligned} L_{m-1}\ \psi_{m-1} &= K^{m}_{m-1}\ \psi_m + K^{m+1}_{m-1}\ \psi_{m+1} \\ L_m\ \psi_m &= K^{m-1}_{m}\ \psi_{m-1} + K^{m+1}_{m}\ \psi_{m+1} \\ L_{m+1}\ \psi_{m+1} &= K^{m-1}_{m+1}\ \psi_{m-1} + K^{m}_{m+1}\ \psi_m \end{aligned} \tag{6}$$

where L and K represent second order radial differential operators.

The solution for the tearing mode perturbation satisfies Eq.(6)

between rational surfaces. At each rational surface ψ_{m-1}, ψ_m and ψ_{m+1} are normally continuous, but discontinuities Δ'_m and Δ'_{m+1} in the logarithmic derivatives of ψ_m and ψ_{m+1} are permitted at their respective resonant surfaces r_m and r_{m+1}. Thus the ideal solutions in the region $0 < r < a$, where a is the edge of the plasma, can be spanned by the following set of basis solutions of Eq.(6). Each solution $\underset{\sim}{\psi}^i$, $1 \leq i \leq 5$ forms a vector

$$\underset{\sim}{\psi}^i = (\psi^i_{m-1}, \psi^i_m, \psi^i_{m+1}) \tag{7}$$

$\underset{\sim}{\psi}^1$, $\underset{\sim}{\psi}^2$ and $\underset{\sim}{\psi}^3$ are linearly independent solutions regular at $r = 0$ and continuous in value and derivative at r_m and r_{m+1}. $\underset{\sim}{\psi}^4$ is defined on $r_m \leq r \leq a$ with $\psi^4_m(r_m) = 0$ and $\psi^{4\prime}_m(r_m) = 1$ and together with its derivative, is continuous at r_{m+1} (as we shall see later, $\psi^4_{m-1}(r_m)$ and $\psi^4_{m+1}(r_m)$ are determined from Eq.(6)). Similarly $\underset{\sim}{\psi}^5$ is defined on $r_{m+1} < r \leq a$ with $\psi^5_{m+1}(r_{m+1}) = 0$ and $\psi^{5\prime}_{m+1}(r_{m+1}) = 1$. ψ^4_m and ψ^5_{m+1} will be recognised as 'small' solutions in the sense of Newcomb.[18] Fig.1 summarises this structure.

In the region $0 \leq r < r_m$ the toroidal tearing mode eigenfunction must be a linear combination of solutions $\underset{\sim}{\psi}^1$, $\underset{\sim}{\psi}^2$ and $\underset{\sim}{\psi}^3$ since these are the only three independent solutions which vanish at the origin. Thus

$$\underset{\sim}{\psi}(r) = \alpha_1\underset{\sim}{\psi}^1(r) + \alpha_2\underset{\sim}{\psi}^2(r) + \alpha_3\underset{\sim}{\psi}^3(r) \tag{8}$$

In the region $r_m \leq r \leq r_{m+1}$ the discontinuity in slope at r_m is introduced by setting

$$\underset{\sim}{\psi}(r) = \alpha_1\underset{\sim}{\psi}^1(r) + \alpha_2\underset{\sim}{\psi}^2(r) + \alpha_3\psi^3(r) + \alpha_4\underset{\sim}{\psi}^4(r) \tag{9}$$

where, from Eq.(2),

$$\alpha_4 = \Delta'_m \psi_m(r_m). \tag{10}$$

with $\psi_m(r_m)$ given by

$$\psi_m(r_m) = \alpha_1 \psi_m^1(r_m) + \alpha_2 \psi_m^2(r_m) + \alpha_3 \psi_m^3(r_m) \tag{11}$$

Similarly in the region $r_{m+1} \leqslant r \leqslant a$

$$\underset{\sim}{\psi}(r) = \alpha_1 \underset{\sim}{\psi}^1(r) + \alpha_2 \underset{\sim}{\psi}^2(r) + \alpha_3 \underset{\sim}{\psi}^3(r) + \alpha_4 \underset{\sim}{\psi}^4(r) + \alpha_5 \underset{\sim}{\psi}^5(r) \tag{12}$$

and

$$\alpha_5 = \Delta'_{m+1} \quad \psi_{m+1}(r_{m+1}) \tag{13}$$

where

$$\psi_{m+1}(r_{m+1}) = \alpha_1 \psi_{m+1}^1(r_{m+1}) + \alpha_2 \psi_{m+1}^2(r_{m+1}) + \alpha_3 \psi_{m+1}^3(r_{m+1})$$

$$+ \alpha_4 \psi_{m+1}^4(r_{m+1}) \tag{14}$$

At the wall, r = a, the boundary condition $\underset{\sim}{\psi}(r) = 0$ holds, so that, in matrix notation,

$$\underset{\approx}{A} \cdot \underset{\sim}{\alpha} = -\underset{\approx}{B} \cdot \underset{\sim}{\alpha}' \tag{15}$$

where

$$\underset{\sim}{\alpha} = \begin{bmatrix} \alpha_1 \\ \alpha_2 \\ \alpha_3 \end{bmatrix} \qquad \underset{\sim}{\alpha}' = \begin{bmatrix} \alpha_4 \\ \alpha_5 \end{bmatrix} \tag{16}$$

$$\underset{\approx}{A} = \begin{bmatrix} \psi^1_{m-1}(a) & \psi^2_{m-1}(a) & \psi^3_{m-1}(a) \\ \psi^1_{m}(a) & \psi^2_{m}(a) & \psi^3_{m}(a) \\ \psi^1_{m+1}(a) & \psi^2_{m+1}(a) & \psi^3_{m+1}(a) \end{bmatrix} \tag{17}$$

and

$$\underset{\approx}{B} = \begin{bmatrix} \psi^4_{m-1}(a) & \psi^5_{m-1}(a) \\ \psi^4_{m}(a) & \psi^5_{m}(a) \\ \psi^4_{m+1}(a) & \psi^5_{m+1}(a) \end{bmatrix} \tag{18}$$

Eqs.(11) and (14) can be expressed as

$$\underset{\approx}{\Delta}' \cdot \underset{\approx}{C} \cdot \underset{\sim}{\alpha} = (\underset{\approx}{I} - \underset{\approx}{\Delta}' \cdot \underset{\approx}{D}) \cdot \underset{\sim}{\alpha}' \tag{19}$$

where

$$\underset{\approx}{\Delta}' = \begin{bmatrix} \Delta'_m & 0 \\ 0 & \Delta'_{m+1} \end{bmatrix} \tag{20}$$

and

$$\underset{\approx}{C} = \begin{bmatrix} \psi_m^1(r_m) & \psi_m^2(r_m) & \psi_m^3(r_m) \\ \psi_{m+1}^1(r_{m+1}) & \psi_{m+1}^2(r_{m+1}) & \psi_{m+1}^3(r_{m+1}) \end{bmatrix} \tag{21}$$

$$\underset{\approx}{D} = \begin{bmatrix} 0 & 0 \\ \psi_{m+1}^4(r_{m+1}) & 0 \end{bmatrix} \tag{22}$$

Eliminating $\underset{\sim}{\alpha}$ between Eqs.(19) and (15) we obtain, assuming $|\underset{\approx}{A}| \neq 0$,

$$\left(\underset{\approx}{I} + \underset{\approx}{\Delta}' \cdot \underset{\approx}{E}\right) \cdot \underset{\sim}{\alpha}' = 0 \tag{23}$$

where $\underset{\approx}{E} = \underset{\approx}{C} \cdot \underset{\approx}{A}^{-1} \cdot \underset{\approx}{B} - \underset{\approx}{D}$. (When $|\underset{\approx}{A}| = 0$, there exists a solution with $\underset{\sim}{\alpha}' = 0$ corresponding to a $\underset{\sim}{\psi}$ which is continuous at r_m and r_{m+1}.) The condition for a non-trivial solution is

$$\left|\underset{\approx}{I} + \underset{\approx}{\Delta}' \cdot \underset{\approx}{E}\right| = 0 \tag{24}$$

Eq.(24), can be written as a relationship

$$(\Delta'_m - \alpha)(\Delta'_{m+1} - \beta) - \gamma = 0 \tag{25}$$

between Δ'_m and Δ'_{m+1}, where

$$\alpha = \frac{-E_{22}}{|\underset{\approx}{E}|}, \quad \beta = \frac{-E_{11}}{|\underset{\approx}{E}|} \quad \text{and} \quad \gamma = \frac{E_{12}E_{21}}{|\underset{\approx}{E}|} \tag{26}$$

Eq.(25) describes a hyperbola in the $\Delta'_{m+1} - \Delta'_m$ plane (shown in Fig.(2)) on which all eigenmodes must lie. Any resonant layer calculation leads to a matching condition

$$\begin{aligned} \Delta'_m &= \Delta_m(\omega) \\ \Delta'_{m+1} &= \Delta_{m+1}(\omega) \end{aligned} \tag{27}$$

where the forms of $\Delta_m(\omega)$ and $\Delta_{m+1}(\omega)$ depend on the resonant layer physics considered. Combining Eq.(25) with Eq.(27) yields a dispersion relation for ω. Graphically, ω can be regarded as parameterising a curve in the $\Delta'_m - \Delta'_{m+1}$ plane through Eq.(27), whose intersections with the hyperbola yield the frequencies of the tearing modes. With the simple form Eq.(3) for $\Delta_m(\omega)$ and $\Delta_{m+1}(\omega)$ this curve is a straight line through the origin and instability corresponds to an intersection in the first quadrant. Simple geometrical considerations imply that the upper branch of the hyperbola does not enter this quadrant if

$$\alpha < 0 \ , \ \beta < 0 \ , \ \alpha\beta > \gamma \tag{28}$$

or $E_{11} > 0 \ , \ E_{22} > 0 \ , \ |\underset{\approx}{E}| > 0$

The result Eq.(28) constitutes a stability criterion for the layer model of Eq.(3). In Appendix B we develop this theory in a formal manner for an arbitrary number of poloidal harmonics and rational surfaces.

For non-linear layer applications it is more convenient to express equation (23) as

$$\left(\underset{\approx}{I} + \underset{\approx}{E} \cdot \underset{\approx}{\Delta}'\right) \cdot \underset{\sim}{W} = 0 \tag{29}$$

where $\underset{\sim}{W}$ can be interpreted in terms of island widths:

$$\underset{\sim}{W} = \begin{bmatrix} \psi_m(r_m) \\ \psi_{m+1}(r_{m+1}) \end{bmatrix} \tag{30}$$

When the size of the island produced at a rational surface is comparable with the linear layer width, non-linear effects become important in the layer. Non-linear layers typically obey equations of the form[19,20]

$$\Delta'_m = \Delta_m\left(\psi_m, \frac{d\psi_m}{dt}\right) \tag{31}$$

and substitution of Eq.(31) into Eq.(29) yields coupled non-linear equations for ψ_m and ψ_{m+1}.

In the following sections we apply the general linear theory to a number of interesting cases. We also describe analytic and numerical techniques for obtaining the information that determines the matrix $\underset{\approx}{E}$ governing the stability of toroidal tearing modes.

III Toroidal Coupling of the m=1 n=1 and m=2 n=1 tearing modes

It is commonly believed that the (m=1, n=1) and (m=2, n=1) tearing modes are particularly significant in a tokamak. The interaction between these modes due to toroidal coupling may well play a role in sawtooth oscillations and disruptions, the most obvious manifestations of mhd activity in a tokamak.

In the tokamak limit of a cylindrical plasma the resistive (m=1, n=1) mode has a particularly large value of Δ'.[21] Indeed Δ'_1 is inversely proportional to the potential energy, δW^C, of the ideal internal kink mode

$$\Delta'_1 \alpha \frac{1}{\delta W^C} \sim \varepsilon^{-2} \tag{32}$$

A similar feature occurs for a large aspect ratio $\beta \sim \varepsilon^2$ tokamak when $\delta W^C \to \varepsilon_1^2 \delta W^T$, where ε_1 is the inverse aspect ratio of the $q = 1$ surface and δW^T, a truly toroidal quantity, involves coupling of m=1 to m=0 and m=2 harmonics.

It is possible to develop a systematic expansion to $0(\varepsilon^2)$ which describes the coupling of the m=1 and m=2 modes and involves the m=0 but excludes the m=3 harmonics. One can then apply the three mode, two resonant surface formulation of Section II directly to this problem.

It should be noted that the 'continuous ψ' approximation implicit in Section II is still valid for the $m=1$ mode, despite the large value for Δ_1' (see Appendix B).

To discuss this problem we require the explicit forms of Eq.(6) for three coupled poloidal harmonics in a large aspect ratio tokamak equilibrium with $\beta \sim \varepsilon^2$. The details of this equilibrium configuration have been given in Ref. 22 and the appropriate marginal ideal mhd equations are derived in Appendix A. The operators L_m, K_m^{m+1} and K_m^{m-1} appearing in Eq.(6) then take the form given in Eqs.(A.18) to (A.20). It should be noted that these equations differ from those of Ref. 17 which did not allow for a perturbation in the toroidal field.

In order to describe the 0, 1 and 2 harmonics we set $m=1$ in Eq.(6) and (A.18-20). As a convenient set we choose the basis functions of Eq.(7), $\underset{\sim}{\psi}^1$, $\underset{\sim}{\psi}^2$ and $\underset{\sim}{\psi}^3$ to be the regular $m=0$, 1 and 2 solutions at $r=0$, $\underset{\sim}{\psi}^4$ to be the small (in the Newcomb sense) $m=1$ solution at the $q=1$ surface and $\underset{\sim}{\psi}^5$ the small $m=2$ solution at the $q=2$ surface. Toroidal coupling, of course, generates other harmonic components in the $\underset{\sim}{\psi}^i$.

The calculation of α, β and γ appearing in relation (25) requires integration of Eq.(6) and (A.18-20). An analytic solution, though rather tedious, is possible because of two special properties of the $m=0$ and $m=1$ Fourier components. To be specific, since the $m=0$ solution regular at the origin is a constant in leading order in ε, it is clear from Eqs.(6) and (A.18-20) that the $m=0$ component does not drive any $m=1$ or $m=2$ harmonics to $0(\varepsilon)$. Furthermore $\psi_1^2(r_1) \sim 0(\varepsilon^2)$, since the regular $m=1$ solution at $r=0$ is $\psi_1^2 = r(1/q - 1)c + 0(\varepsilon^2)$ where c

is a constant, and thus is almost entirely the small solution at $q=1$. The remaining quantities needed can be calculated analytically by integration of Eqs.(6,A.18-20) with appropriate boundary conditions. Since the result is not novel we do not reproduce the details.

We find that relation (25) can be expressed in the compact and physically meaningful form used in Ref. 15.

$$\left(\frac{1}{r_1\Delta_1'} - \varepsilon_1^2\frac{\delta W^T}{s_1^2}\right) r_2\left(\Delta_2' - \Delta_2'^{c}\right) + \varepsilon_1^2\left(\frac{\delta W_{12}}{s_1}\right)^2 = 0 \qquad (33)$$

Here $\varepsilon_1^2\delta W^T$ is the potential energy of the ideal internal kink mode[23]

$$\delta W^T = \frac{8\sigma(b-c) + 9/4(b-1)(1-c) - 6(b-1)(c+3)(\beta_p+\sigma) - 4(c+3)(b+3)(\beta_p+\sigma)^2}{16\,(b-c)} \qquad (34)$$

$\Delta_2'^{c}$ is the cylindrical Δ' for the $m=2$ mode, δW_{12} is a coupling integral

$$\delta W_{12} = \frac{1}{2}\,\frac{\psi_-(r_1)}{\psi_-(r_2)}\left[(\beta_p + \sigma)(b+3) + \frac{3}{4}(b-1)\right] \qquad (35)$$

where

$$\beta_p = \frac{2}{B_\theta^2(r_1)}\int_0^{r_1}\frac{dr}{r_1}\frac{dp}{dr}\left(\frac{r}{r_1}\right)^2, \quad \sigma = \int_0^{r_1}\frac{dr}{r_1}\left(\frac{r}{r_1}\right)^3\left(\frac{1}{q^2} - 1\right) \qquad (36)$$

$$s_1 = (r/q)(dq/dr)_{r = r_1}, \qquad \varepsilon_1 = {}^{r_1}/_{R}, \tag{37}$$

and the quantities b and c are given by

$$b = r\,\frac{d}{dr}\ln \xi_-\Big|_{r_{1-}} \qquad c = r\,\frac{d}{dr}\ln \xi_+\Big|_{r_{1+}} \tag{38}$$

with $\xi_\pm = \left[r\left(1/q - 1/2\right)\right]^{-1}\psi_\pm$, where ψ_- is a cylindrical m=2 solution vanishing at r=0 and ψ_+ one vanishing at q=2.

The structure of the relation Eq.(33) between Δ_1' and Δ_2' depends on the parameters $\Delta_2'^{c}$, $\varepsilon_1^2\delta W^T/s_1^2$ and $\varepsilon_1^2(\delta W_{12})^2/s_1^2$. The eigenvalue equations result from inserting appropriate layer models for Δ_1' and Δ_2'. Rewriting Eq.(33) in the form of Eq.(25),

$$\left(r_1\Delta_1' - \frac{s_1^2}{\varepsilon_1^2\delta W^T}\right)\left(r_2\Delta_2' - r_2\Delta_2'^{c} - \frac{\delta W_{12}^2}{\delta W^T}\right) - \left(\frac{s_1}{\varepsilon_1}\frac{\delta W_{12}}{\delta W^T}\right)^2 = 0 \tag{39}$$

we can identify analytic expressions for α, β and γ. Eq.(39) indicates that, at least for resistive layers (3), coupling of the m=1 and m=2 tearing modes is unimportant, although coupling to an m=2 Fourier component is an important ingredient in the calculation of δW^T and therefore in the stability of the m=1 resistive mode. For typical tokamak parameters, and a simple resistive layer, the 'm=1 mode' is unstable with a growth rate scaling as $S^{-1/3}$ when $q_0 < 1$. However as observed in Ref.15, Eq.(39) also suggests that at tight aspect ratio and for low shear at the q=1 surface, coupling of the m=2 and m=1

tearing modes should become significant. Nevertheless an unstable resistive tearing mode remains in a large aspect ratio tokamak even when $\delta W^T > 0$ (i.e. the ideal internal kink is stable), since the hyperbola (39) still has at least one branch in the first quadrant.

IV Two Coupled Tearing Modes

In this section we consider the toroidal coupling of two tearing modes, m and m+1, in a large aspect ratio tokamak. We can again apply the formalism of Section II for three modes and two resonant surfaces so that the m-1 harmonic is non-resonant. The relevant equations for the large aspect ratio tokamak are again (A16-A20) of Appendix A.

The relation (25) between Δ'_m and Δ'_{m+1} will, in general, approximately decouple into $\Delta'_m = \alpha$, $\Delta'_{m+1} = \beta$ since the coupling term $\gamma \sim \varepsilon^2$. However a significant interaction between m and m+1 will occur if either α or $\beta \sim \varepsilon^2$ or if $\alpha \sim \beta \sim \varepsilon$. We focus on this latter situation and obtain a dispersion relation involving coupling integrals in terms of the m and m+1 cylindrical tearing mode solutions.[16]

Again we define solution $\underset{\sim}{\psi}^1$ to be pure m+1 harmonic at the origin, $\underset{\sim}{\psi}^2$ to be pure m and $\underset{\sim}{\psi}^3$ entirely m-1, while $\underset{\sim}{\psi}^4$ and $\underset{\sim}{\psi}^5$ are the small m and m+1 solutions starting from r_m and r_{m+1}, respectively. Clearly cylindrical values of Δ' obey the relations

$$\psi_m^2(a) + \Delta'^c_m \, \psi_m^2(r_m) \, \psi_m^4(a) = 0 \tag{40}$$

$$\psi_{m+1}^1(a) + \Delta'^c_{m+1} \, \psi_{m+1}^1(r_{m+1}) \, \psi_{m+1}^5(a) = 0 \tag{41}$$

so that the case we are considering corresponds to a special ordering

$\psi_m^2(a) \sim \psi_{m+1}^1(a) \sim \varepsilon$. This is complemented by the results

$$\psi_m^1(r) \sim \psi_m^3(r) \sim \psi_m^5(r) \sim \varepsilon \ , \quad \psi_m^2(r\neq a) \sim \psi_m^4(r) \sim 1 \ ;$$

$$\psi_{m+1}^1(r\neq a) \sim \psi_{m+1}^5(r) \sim 1 \ , \quad \psi_{m+1}^2(r) \sim \psi_{m+1}^4(r) \sim \varepsilon \ , \quad \psi_{m+1}^3 \sim \varepsilon^2 \ ; \tag{42}$$

$$\psi_{m-1}^1(r) \sim \psi_{m-1}^5(r) \sim \varepsilon^2 \ , \quad \psi_{m-1}^2(r) \sim \psi_{m-1}^4(r) \sim \varepsilon \ , \quad \psi_{m-1}^3(r) \sim 1$$

generated by the couplings in Eq.(6) and Eq.(A.18-20).

Inserting this ordering into the relation (25) results in

$$(\Delta_m' - \Delta_m'^{\,c})(\Delta_{m+1}' - \Delta_{m+1}'^{\,c}) = I_1 I_2 \tag{43}$$

where

$$I_1 = \frac{\psi_{m+1}^2(a)}{\psi_{m+1}^1(r_{m+1})\ \psi_{m+1}^5(a)} \ , \qquad I_2 = \frac{\psi_m^1(a)}{\psi_m^2(r_m)\ \psi_m^4(a)} \tag{44}$$

$\psi_m^1(a)$ and $\psi_{m+1}^2(a)$ can be evaluated by solving Eq.(6) and Eq.(A.18-20) using the method of variation of parameters. This requires solutions to the homogeneous equations for ψ_m^2 and ψ_{m+1}^1 which are of course cylindrical equations. As the two independent homogeneous solutions in each case we choose one vanishing at $r=0$ and the other at $r=a$. The resulting integral expressions for $\psi_m^1(r)$ and $\psi_{m+1}^2(r)$ involve a principal part prescription at the resonant radii r_m and r_{m+1} respectively. [The apparent second order poles in the integrands arising from pressure gradient terms in Eqs.(A.18-20) are reduced to first order

by cancellation of the numerators at the resonant points.] These provide expressions for I_1 and I_2 (which are related by the self-adjointness property of the ideal mhd equations) leading to

$$(\Delta'_m - \Delta'^{c}_m)(\Delta'_{m+1} - \Delta'^{c}_{m+1}) = I^2 \tag{45}$$

$$I = \frac{1}{\psi_m(r_m)\psi_{m+1}(r_{m+1})} \left\{ \int_0^a dr \left[r\Delta' \psi'_m \psi'_{m+1} \right.\right.$$

$$+ \frac{1}{2}\left(r\Delta'' + \Delta' + \frac{r}{R}\right)\left((m+1)\psi'_m\psi_m - m\psi_m\psi'_{m+1}\right)$$

$$\left. - \frac{m(m+1)}{r}\left(\Delta' + \frac{r}{2R}\right)\psi_m\psi_{m+1}\right]$$

$$\left. + P\int_0^a dr \frac{Rp'q}{rB^2}\left[\frac{r\,\psi'_m\psi_{m+1}}{\left(\frac{1}{q} - \frac{n}{m+1}\right)} + \frac{r\,\psi_m\psi'_{m+1}}{\left(\frac{1}{q} - \frac{n}{m}\right)} + \frac{1}{q}\frac{(1+s)\psi_m\psi_{m+1}}{\left(\frac{1}{q} - \frac{n}{m}\right)\left(\frac{1}{q} - \frac{n}{m+1}\right)}\right]\right\} \tag{46}$$

where P denotes a principal part integration, ψ_m and ψ_{m+1} are the cylindrical tearing mode eigenfunctions, prime denotes a radial derivative and Δ' is the conventional notation for the Shafranov shift. In this expression ψ_m is defined in the range $0 \leq r \leq r_m$ as the cylindrical solution which vanishes at $r=0$ and in the range $r_m \leq r \leq a$ as the one which vanishes at $r=a$, and similarly for ψ_{m+1}. Because Δ'_m and Δ'_{m+1} are $0(\varepsilon)$, ψ_m and ψ_{m+1} have almost continuous derivatives at r_m and r_{m+1} respectively. The result, Eq.(46), is a finite pressure ($\beta_p \sim 1$)

generalisation of that given in Ref. 16, and can be computed using only cylindrical solutions.

The only toroidal effect in Eq.(45) is the quantity I which measures the displacement of the hyperbola from the cylindrical asymptotes. Since $I^2 > 0$ this displacement produces a branch of the hyperbola in the upper righthand quadrant relative to these asymptotes. At least for the simple layer model (3) we can conclude therefore that toroidicity has a destabilising influence in this limit.

V Toroidal Coupling of Tearing Modes at Finite Pressure

The Eqs.(6) with the results (A.16)-(A.20) can be used to investigate the effect of toroidal coupling in the presence of a finite pressure gradient. Indeed, for simplicity, we retain only toroidal effects due to pressure, i.e. we assume $\varepsilon < \varepsilon\beta_p < \varepsilon^{1/3}$ where the upper limit allows us to ignore coupling to elliptic distortion of the magnetic surfaces induced by pressure.[24] Eqns.(A19)-(A20) describing the L_2 and K operators then simplify:

$$K_m^{m+1}\psi_{m+1} = \frac{d}{dr}\left[r\Delta' \frac{d\psi_{m+1}}{dr}\right] + \frac{m(m+1)}{r}\Delta'\psi_{m+1} + \frac{m+1}{2}\frac{d}{dr}\left[(r\Delta'' + \Delta')\psi_{m+1}\right]$$

$$+ \frac{m}{2}(r\Delta'' + \Delta')\frac{d\psi_{m+1}}{dr} + r\frac{d}{dr}\left[\frac{Rp'q}{rB_0^2}\right]\frac{(m+1)q\psi_{m+1}}{(m+1-nq)}$$

$$- \frac{Rp'q}{B_0^2}\frac{nq}{m-nq}\frac{d}{dr}\left[\frac{q\psi_{m+1}}{m+1-nq}\right] - \frac{Rp'q}{B_0^2}\frac{\psi_{m+1}}{r}\frac{(m+1)nq^2}{(m-nq)(m+1-nq)}, \tag{47}$$

$$K_m^{m-1}\psi_{m-1} = \frac{d}{dr}\left[r\Delta' \frac{d\psi_{m-1}}{dr}\right] + \frac{m(m-1)}{r}\Delta'\psi_{m-1} - \frac{m-1}{2}\frac{d}{dr}\left[(r\Delta'' + \Delta')\psi_{m-1}\right]$$

$$- \frac{m}{2}\left(r\Delta'' + \Delta'\right)\frac{d\psi_{m-1}}{dr} + r\frac{d}{dr}\left[\frac{Rp'q}{rB_0^2}\right]\frac{(m-1)q\ \psi_{m-1}}{(m-1-nq)}$$

$$+ \frac{Rp'q}{B_0^2}\frac{nq}{(m-nq)}\frac{d}{dr}\left[\frac{q\ \psi_{m-1}}{m-1-nq}\right] - \frac{Rp'q}{B_0^2}\frac{\psi_{m-1}}{r}\frac{nq^2(m-1)}{(m-nq)(m-1-nq)}, \tag{48}$$

$$L_{m2}\ \psi_m = \frac{d}{dr}\frac{r}{2}\Delta'^2\frac{d\psi_m}{dr} - \frac{2\psi_m}{(m-nq)^2}\frac{m^2q^2}{r}\frac{Rp'q}{B_0^2}\left[\frac{Rp'q}{B_0^2} + r\left(\frac{1}{q}\right)'\Delta'\right]$$

$$+ \frac{\psi_m\, mq}{(m-nq)}\frac{d}{dr}\left\{2\Delta'\frac{Rp'q}{B_0^2} + \frac{2\Delta'^2}{q} + \frac{3}{2}r\left(\frac{1}{q}\right)'\Delta'^2\right\}$$

$$- \psi_m\frac{m^2}{r}\left[2\Delta'^2 + \frac{1}{2}r\Delta''\left(r\Delta'' + 2\Delta'\right)\right] \tag{49}$$

It is evident that the pressure gradient introduces higher order singularities near the resonant surfaces than occur in the absence of pressure (or in the cylindrical limit). The nature of the singularities can be understood by expanding the equations around the resonant surfaces r_{m+1}, r_m and r_{m-1}. We find that near the surface r_m the solutions behave as

$$\psi_m \sim x^p \qquad x = r - r_m \tag{50}$$

where $p(p-1) \sim 0[(\varepsilon\beta_p)^4]$, consistent with Ref. 24. Thus the Mercier indices[12] are $p_+ \simeq 1$ and $p_- \simeq 0$ since our equations are accurate only to $0[(\varepsilon\beta_p)^2]$. As computation is simplified by having $p_+ = 1$ and $p_- = 0$ exactly, we add an $0[(\varepsilon\beta_p)^4]$ term to L_m to ensure that this is so; this modification will not have any other significant effect on the solutions. Near the other surfaces $r_{m\pm1}$, however, we find

$$\psi_{m\pm1} \sim x^p \qquad x = r - r_{m\pm1} \tag{51}$$

where $p(p-1) \sim 0[(\varepsilon\beta_p)^2]$, inconsistent with the correct result.[24] This is because the truncation at three harmonics leads to a lack of symmetry between r_m and $r_{m\pm1}$ which can only be recovered by including $m\pm2$ harmonics. By examining the influence of these near the resonant surfaces $r_{m\pm1}$ we find that their effect on the Mercier indices can be simulated by appropriate modifications of $L_{m\pm1}$ in $0[(\varepsilon\beta_p)^2]$, with the result

that Eq.(51) is replaced by the correct form. Further modification of $L_{m\pm1}$ in $0[(\varepsilon\beta_p)^4]$ again ensures $p_+ = 1$ and $p_- = 0$ exactly. The details of these modifications will appear in a later publication.

The resulting equations have been solved numerically. The three second order equations are first written as a set of six first order equations for ψ_k, $u_k = r\psi_k'$, with $k = m-1$, m, and $m+1$. The three basis solutions $\underset{\sim}{\psi}^1$, $\underset{\sim}{\psi}^2$ and $\underset{\sim}{\psi}^3$ correspond to the following boundary conditions at $\rho = r/a = 0$.

$$\psi_m^1 = \rho^m,\ u_m^1 = m\rho^m,\ \psi_{m+1}^1 = 0,\ u_{m+1}^1 = 0,\ \psi_{m-1}^1 = 0,\ u_{m-1}^1 = 0$$

$$\psi_{m-1}^2 = \rho^{m-1},\ u_{m-1}^2 = (m-1)\rho^{m-1},\ \psi_{m+1}^2 = 0,\ u_{m+1}^2 = 0,\ \psi_m^2 = 0,\ u_m^2 = 0$$

$$\psi_{m+1}^3 = \rho^{m+1},\ u_{m+1}^3 = (m+1)\rho^{m+1},\ \psi_{m-1}^3 = 0,\ u_{m-1}^3 = 0,\ \psi_m^3 = 0,\ u_m^3 = 0 \qquad (53)$$

However the resulting equations for u_k' are driven by combinations of terms which, individually, are singular as $(\rho - \rho_{m-1})^{-2}$ near the resonant surface ρ_{m-1} but cancel to produce a weaker singularity $\sim(\rho - \rho_{m-1})^{-1}$. It eases the numerical integration near ρ_{m-1} to achieve this cancellation analytically rather than numerically by introducing, in place of u_{m+1} and u_m, quantities which make it explicit. Thus we switch to new dependent variables at a point ρ_1 before reaching ρ_{m-1}, to further new variables at a point ρ_2 between ρ_{m-1} and ρ_m and finally to yet further ones at a point ρ_3 between ρ_m and ρ_{m+1}. These rather tedious details will be described fully in the later publication. The results are of course independent of the precise positions of ρ_1, ρ_2 and ρ_3 as has been verified numerically.

With these procedures the equations have been integrated by a shooting method and the quantities $\psi_m(1)$ $\psi_{m-1}(1)$ and $\psi_{m+1}(1)$, which contain the information for constructing the hyperboloids, evaluated. In particular we show in Fig.3 the hyperbola for Δ_2' and Δ_3' for a case with a q profile given by $q = 1.1(1 + 2\rho^2)$, possessing two rational surfaces when $n=1$, and a pressure profile $p = p_0(1 - \rho^2)$ with $\beta_0 R/a = 0.08$ where $\beta_0 = 2p_0/B^2$. As an illustration we have used the simple resistive mhd layer theory of Eq.(3) and, assuming the resistivity

profile varies inversely with the current profile, have calculated the variation in growth rate with $\beta_0 R/a$ the results being shown in Fig. 4. This shows that increasing toroidal coupling due to pressure gradients further destablises the $m=2$ cylindrical tearing mode. In fact the asymptotes of the hyperbola $\Delta'_m = \alpha$ and $\Delta'_{m+1} = \beta$ both show destabilising trends as $\beta_0 R/a$ is increased, in addition to the destabilisation inherent in γ as discussed earlier in the context of I^2 of Eq.(45).

VI The Use of Initial Value Resistive MHD Codes to Compute the "Toroidal Δ'"

Recently several codes have been developed which solve the resistive mhd equations in full toroidal geometry with no ordering assumptions.[10,11] These codes have been very successful in studying a range of problems. However they implicitly treat the resonant layers in a simple resistive mhd approximation which is, of course, inappropriate for a high temperature plasma. In this section we describe a method of extending the validity of these codes to a more realistic description of the resistive layer.

We exploit our understanding of the structure of the toroidal tearing mode eigenvalue problem described in Section II to obtain the structure of relation (4) from the output of an initial value resistive mhd code. To elucidate the method we consider a situation with two rational surfaces labelled by m and $m+1$ so that our objective is to determine α, β and γ which relate Δ'_m and Δ'_{m+1} in Eq.(25). Since we employ a resistive mhd code these quantities must match the corresponding quantities $\Delta_m(\omega)$ and $\Delta_{m+1}(\omega)$ appropriate to resistive mhd layer models at the two

resonant surfaces (given by Eq.(3) at low β or the finite β formulation discussed by Glasser et al in Ref. 12). A calculation with an initial value resistive mhd code for a particular equilibrium and a given resistivity profile $\eta(r)$ will yield a tearing mode frequency ω, though only the values of η near the two rational surfaces affect the value of ω. Then evaluating $\Delta_m(\omega)$ and $\Delta_{m+1}(\omega)$ for the appropriate resistive mhd layer model, equating them to Δ'_m and Δ'_{m+1} respectively and substituting them into Eq.(25) provides one equation for α, β and γ. Two more relations can be obtained by repeating the process for two different resistivity profiles, while retaining the same mhd equilibrium. These three relations are sufficient to determine α, β and γ. Geometrically the procedure is equivalent to finding three points on a hyperbola, which are then sufficient to construct the whole curve. As a check on the accuracy of the method the resistivity profile can be varied once more to confirm that the values obtained for α, β and γ produce the correct eigenfrequency. The essence of the method is that changing the resistivity profile affects the layer response and the eigenvalue but not the values of α, β and γ which are determined by ideal mhd properties. Of course the equations used in the initial value code should reduce to the marginal ideal mhd equations outside the layer. Furthermore the form they take in the resistive layer should allow ω to be sensitive to Δ' and not to be completely dominated by the properties of the layer.

To test the method we have used the initial value code FAR,[11] which solves the incompressible resistive mhd equations in full toroidal geometry, with no ordering assumptions. The equilibrium for the case described here, has an aspect ratio of 10, zero β, and a current profile as shown in Fig. 5 with $1.3 \leq q \leq 3.6$. For this situation the layer

results $\Delta(\omega)$ are given by Eq.(3). The hyperbola relating Δ_2' and Δ_3' for this equilibrium, which can be expressed as

$$(\Delta_2' - 7.11)(\Delta_3' - 8.73) - 0.45 = 0, \tag{53}$$

is shown in Fig. 6. The crosses in this figure are the three points determined in the manner described above and used to fit the hyperbola, while the open circles are determined using other profiles of resistivity $\eta(r)$; the extent to which they lie on the hyperbola is a test of the validity of the method. We are able to obtain points on the lower left branch of the hyperbola because the FAR code can also calculate subdominant eigenvalues.[10] The greater deviation of data points from the lower hyperbola is almost certainly related to the increased difficulty in obtaining converged results for these subdominant eigenvalues. We note that the equivalent cylindrical equilibrium yields $\Delta_2' = 7.15$ and $\Delta_3' = 9.1$ and thus the asymptotes have decreased slightly due to the toroidal effects. However the toroidal coupling effect arising from $\gamma = 0.45$ is destabilising. The net toroidal effect on stability is seen to be a competition between these two opposing effects so that no general conclusion can be drawn.

It is clear from Fig. 5 that the case considered above had a current profile with 'shoulders' in order to make both asymptotes positive. This allowed us to examine the structure of both branches of the hyperbola with the initial value code, whose range for growing solutions is limited to the upper right quadrant of the $\Delta_2' - \Delta_3'$ plane. However the Δ_3' asymptote is negative for more typical tokamak equilibria and we are presently examining methods of extending the range of the FAR code in the $\Delta_2' - \Delta_3'$ plane. We also avoided many of the problems associated with

evaluating the average curvature etc., in the dispersion relation of Ref. 12 by considering the case of zero β; for finite β these quantities will also require numerical evaluation. Finally we note that although we have only considered a two rational surface case the extension of the method to three or more surfaces is straight forward.

VII Discussion and Conclusions

In Section II we discussed the general structure of the axisymmetric toroidal tearing mode problem for those circumstances in which it can be separated into a matching problem between marginal ideal mhd solutions and resonant layer solutions. This discussion was simplified for clarity but possessed the essential features of the more detailed analysis in Appendix B which resembles the approach employed in Resistive PEST.[14] For k resonant surfaces our description of the ideal mhd aspect leads to a single relation (a k-dimensional hyperboloid) between the k quantities Δ'_k representing discontinuities at those surfaces. Insertion of realistic resonant layer expressions into the matching conditions $\Delta'_k = \Delta_k(\gamma)$ then leads to the appropriate dispersion relation for the growth rate γ. In this paper we have emphasized the structure of the ideal mhd aspect and discussed procedures for calculating the appropriate quantities defining the hyperboloid.

In particular, as an illustration, we have described the example of three poloidal fourier harmonics, $m-1$, m and $m+1$, with two resonant surfaces at r_m and r_{m+1}, a situation relevant to a large aspect ratio tokamak - in this case a simple graphical representation of the hyperbola for Δ'_m and Δ'_{m+1} is instructive.

The toroidal coupling of the important $(m=1, n=1)$ and $(m=2, n=1)$ modes (a situation previously discussed in Ref.15) is covered by this

case. Because of the typically large values of $\Delta'_1 \sim \varepsilon^{-2}$ there can be a strong interaction between the two modes when there is low shear at the $q=1$ surface even though $\varepsilon << 1$, as shown in Section III. For other pairs of tearing modes the coupling is weak unless Δ'_m and Δ'_{m+1} are both $0(\varepsilon)$, In Section IV we obtained a semi-analytic description of the properties of the hyperbola for such a case. This involves coupling integrals over cylindrical eigenfunctions and generalises the results of Ref.16 to finite pressure. Toroidicity is seen to be destabilising in this limit. More generally we must resort to numerical solution of the ideal mhd equations and in Section V we give an interesting example involving finite pressure gradients. This feature introduces additional singularities at the resonant surfaces and we have manipulated the equations in such a way that a numerical shooting scheme can be used successfully. An example of the stabilising influence of finite pressure is given.

These examples have all referred to a large aspect ratio tokamak equilibrium. Though conceptually easy and in some ways practically relevant, this is clearly not entirely adequate. Nevertheless, our formulation has indicated how one might use initial value resistive mhd codes in realistic geometry to deduce the information needed for our hyperboloids, as described in Section VI. This can then be used in conjunction with realistic representations of the physics in the resonant layer to provide a correct description of tearing modes in a torus. An example, using a finite aspect ratio, low β equilibrium, is given to illustrate the construction of the hyperbola in a case with two resonant surfaces. In this example it was seen that the net effect of toroidicity on stability arose as a competition between stabilising effects from α

and β and a destabilising effect from γ so that a general conclusion cannot be drawn.

In summary we have described the structure of the asymptotic matching approach to tearing modes in an axisymmetric torus. We have given a number of illustrations of the calculation of those properties of the ideal mhd solutions needed to discuss this problem. These techniques, combined with a realistic model for the physics in the resonant layer, provide the equipment for a complete solution of the tearing mode stability of a toroidal plasma.

Appendix A

Marginal Ideal MHD Equations

In this appendix we derive the linearised marginal ideal mhd equations, displaying both the exact equations in the appropriate coordinates and the large aspect ratio limit of these equations retaining corrections to second order in the inverse aspect ratio.

The coordinate system, r, θ, ϕ, where ϕ is the toroidal angle, θ is an angle like variable in the poloidal plane and r is a flux surface label with dimensions of length, is chosen so that the magnetic field lines appear straight. The Jacobian for these coordinates is given by[23]

$$J = \frac{rR^2}{R_0} \tag{A.1}$$

where R is the major radius and R_0 is a conveniently chosen average major radius. The axisymmetric equilibrium magnetic field satisfies $\nabla p = \underset{\sim}{J} \times \underset{\sim}{B}$ so it can be written

$$\underset{\sim}{B} = B_0 R_0 \left[f(r) \ \nabla\phi \times \nabla r + g(r) \ \nabla\phi \right] . \tag{A.2}$$

The safety factor, the slope of the field lines in the $\theta - \phi$ plane is then given by,

$$q(r) = \frac{rg(r)}{R_0 f(r)} . \tag{A.3}$$

The equilibrium Grad-Shafranov equation takes the form

$$\frac{1}{r}\frac{\partial}{\partial r}\left(rf\left|\nabla r\right|^2\right) + \frac{1}{r}\frac{\partial}{\partial \theta}\left(rf\ \nabla\theta\cdot\nabla r\right) + \left(\frac{gg'}{f} + \frac{R^2}{R_0^2}\frac{p'}{B_0^2 f}\right) = 0\ , \qquad (A.4)$$

where primes denote differentiation with respect to r.

Assuming that an axisymmetric equilibrium solution of Eq.(A.4) has been obtained, we consider ideal perturbations of this equilibrium with toroidal mode number n satisfying $\nabla p = \underset{\sim}{J} \times \underset{\sim}{B}$. We eliminate the poloidal and radial perturbed magnetic field by some lengthy algebra and we obtain the coupled equations,

$$\frac{\partial}{\partial r}\left[\left(\frac{\partial}{\partial \theta} - inq\right)y\right] = \frac{\partial}{\partial \theta}\left[Q\frac{\partial z}{\partial \theta}\right] + Sz - \frac{\partial}{\partial \theta}\left[T\left(\frac{\partial}{\partial \theta} - inq\right)y + Uy\right] \qquad (A.5)$$

and

$$\left(\frac{\partial}{\partial \theta} - inq\right)\frac{\partial z}{\partial r} = -\left(\frac{\partial}{\partial \theta} - inq\right)T^*\frac{\partial z}{\partial \theta} + U\frac{\partial z}{\partial \theta} - \left(\frac{\partial}{\partial \theta} - inq\right)V\left(\frac{\partial}{\partial \theta} - inq\right)y$$

$$+ W\left(\frac{\partial}{\partial \theta} - inq\right)y + Xy \qquad (A.6)$$

for the dependant variables $y = R_0 f\ \underset{\sim}{\xi}\cdot\nabla r$ and $z = R^2\delta\underset{\sim}{B}\cdot\nabla\phi/B_0$ where $\underset{\sim}{\xi}$ and $\delta\underset{\sim}{B}$ are the displacement and perturbed magnetic field respectively. Q, S, T, U, V, W and X are equilibrium quantities (with T^* being the complex conjugate of T)

$$Q = \frac{R_0}{in\ r|\nabla r|^2}$$

$$S = \frac{in\ r}{R_0}$$

$$T = \frac{\nabla\theta\cdot\nabla r}{|\nabla r|^2} - \frac{1}{in}\frac{R_0}{r}\frac{g'}{f|\nabla r|^2}$$

$$U = \frac{1}{|\nabla r|^2}\frac{p'}{B_0{}^2 f^2}\frac{R^2}{R_0{}^2}$$

$$V = \frac{R_0}{r|\nabla r|^2}\left[\frac{in}{R^2} + \frac{1}{in}\left(\frac{g'}{f}\right)^2\right]$$

$$W = 2\frac{g'}{f}\frac{p'}{B_0{}^2 f^2}\frac{1}{|\nabla r|^2}\frac{R^2}{R_0{}^2} - \frac{\partial}{\partial r}\left(\frac{g'}{f}\right)$$

$$X = \frac{in\ p'}{B_0{}^2 f^2}\left(\frac{r}{R_0}\right)\left[\frac{\partial}{\partial\theta}\left(T^*\frac{R^2}{R_0{}^2}\right) + \frac{\partial}{\partial r}\left(\frac{R^2}{R_0{}^2}\right) - \frac{R^2}{R_0{}^2}\left(\frac{r}{f}\right)\frac{\partial}{dr}\left(\frac{f}{r}\right) - U\frac{R^2}{R_0{}^2}\right] \qquad (A.7)$$

An important observation is that Eqs.(A.5) and (A.6) are both first order differential equations in the radial variable.

In many cases it is more convenient to write Eqs.(A.5) and (A.6) as an infinite coupled set of equations for the poloidal fourier harmonics. Each poloidal fourier harmonic obeys an equation of the form.

$$\frac{\partial}{\partial r}\left[m - nq)y_m\right] = \sum_{k=-\infty}^{\infty}\left\{B^k{}_m z_k + C^k{}_m y_k\right\} \qquad (A.8)$$

$$(m - nq)\frac{\partial z_m}{dr} = \sum_{k=-\infty}^{\infty} \{ D^k{}_m z_k + E^k{}_m y_k \} \qquad (A.9)$$

where the coefficients B^k_m, C^k_m, D^k_m and E^k_m can be derived in a straight forward manner from Eqs.(A.5), (A.6) and (A.7).

In a large aspect ratio (i.e. $\varepsilon = r/R << 1$) tokamak equilibrium with circular surfaces and $\beta \sim 0(\varepsilon^2)$[22]

$$|\nabla r|^2 = 1 - 2\Delta'\cos\theta + \left(\frac{\Delta'^2}{2} + \frac{3}{4}\frac{r^2}{R_0^2} + \frac{\Delta}{R_0}\right) + 0(\varepsilon^3) , \qquad (A.10)$$

$$\nabla r . \nabla\theta = \frac{1}{r}\left(r\Delta'' + \Delta' + \frac{r}{R_0}\right)\sin\theta + 0(\varepsilon^3) , \qquad (A.11)$$

$$\frac{R^2}{R_0^2} = 1 - \frac{2r}{R_0}\cos\theta - \left(\frac{2\Delta}{R_0} + \frac{r\Delta'}{R_0} + \frac{1}{2}\frac{r^2}{R_0^2}\right) + 0(\varepsilon^3) , \qquad (A.12)$$

$$\Delta'' = \frac{1}{R_0} - \frac{2R_0}{r}\frac{p'}{B_0^2}q^2 - \left[\frac{3}{r} + 2q\left(\frac{1}{q}\right)'\right]\Delta' \qquad (A.13)$$

The two arbitrary functions $p'(r)$ and $q(r)$ specify the equilibrium and $\Delta(r)$ is obtained from Eq.(A.13). In lowest order the Grad-Shafranov equation yields $g = 1 + 0(\varepsilon^2)$, since $f \sim 0(\varepsilon)$ and $p'/B_0^2 \sim 0(\varepsilon^2)$. To $0(\varepsilon^2)$ Eqs.(A.8) and (A.9) simplify since

$$B^m_m , \quad C^m_m , \quad D^m_m , \quad E^m_m \sim 0(1)$$

$$B^{m\pm1}_m , \quad C^{m\pm1}_m , \quad D^{m\pm1}_m , \quad E^{m\pm1}_m \sim 0(\varepsilon) \qquad (A.14)$$

After some lengthy algebra using Eq.(A.4), we obtain from Eqs.(A.8) and (A.9),

$$L_{m0}\ \psi_m + L_{m2}\ \psi_m = K_m^{m+1}\ \psi_{m+1} + K_m^{m-1}\ \psi_{m-1} \tag{A.15}$$

where

$$\psi_m = (m - nq)y_m \tag{A.16}$$

and the operators L_m, L_{m2}, K_m^{m+1} and K_m^{m-1} are defined by

$$L_{m0}\ \psi_m = \frac{d}{dr}\left[r\frac{d\psi_m}{dr}\right] - \frac{m^2}{r}\ \psi_m - \frac{mq\ \psi_m}{(m - nq)}\ \frac{d}{dr}\left(\frac{1}{r}\frac{d}{dr}\frac{r^2}{q}\right), \tag{A.17}$$

$$K_m^{m+1}\psi_{m+1} = \frac{d}{dr}\left[r\Delta'\frac{d\psi_{m+1}}{dr}\right] + \frac{m(m+1)}{r}\left(\Delta' + \frac{r}{R_0}\right)\psi_{m+1} + \frac{m+1}{2}\frac{d}{dr}\left[\left(r\Delta'' + \Delta' + \frac{r}{R_0}\right)\psi_{m+1}\right]$$

$$+ \frac{m}{2}\left(r\Delta'' + \Delta' + \frac{r}{R_0}\right)\frac{d\psi_{m+1}}{dr} + r\frac{d}{dr}\left[\frac{R_0p'q}{rB_0^2}\right]\frac{(m+1)q\ \psi_{m+1}}{(m+1 - nq)}$$

$$- \frac{R_0p'q}{B_0^2}\frac{nq}{(m - nq)}\frac{d}{dr}\left[\frac{q\psi_{m+1}}{(m+1 - nq)}\right] - \frac{R_0p'q}{B_0^2}\frac{\psi_{m+1}}{r}\frac{nq(m+1)q}{(m - nq)(m+1 - nq)}, \tag{A.18}$$

$$K_m^{m-1}\psi_{m-1} = \frac{d}{dr}\left[r\Delta'\frac{d\psi_{m-1}}{dr}\right] + \frac{m(m-1)}{r}\left(\Delta' + \frac{r}{R_0}\right)\psi_{m-1} - \frac{m-1}{2}\frac{d}{dr}\left[\psi_{m-1}\left(r\Delta'' + \Delta' + \frac{r}{R_0}\right)\right]$$

$$- \frac{m}{2}\left(r\Delta'' + \Delta' + \frac{r}{R_0}\right)\frac{d\psi_{m-1}}{dr} + r\frac{d}{dr}\left[\frac{R_0 p' q}{rB_0^2}\right]\frac{(m-1)q\ \psi_{m-1}}{(m-1-nq)}$$

$$+ \frac{R_0 p' q}{B_0^2}\frac{nq}{(m-nq)}\frac{d}{dr}\left[\frac{q\ \psi_{m-1}}{(m-1-nq)}\right] - \frac{R_0 p' q}{B_0^2}\frac{\psi_{m-1}}{r}\frac{nq(m-1)q}{(m-nq)(m-1-nq)}$$

(A.19)

and finally

$$L_{m2}\psi_m = \frac{d}{dr}\left\{\left[\frac{1}{2}\Delta'^2 + \frac{\Delta}{R_0} + \frac{r^2}{R_0^2}\left(\frac{3}{4} - \frac{n^2}{m^2}\right)\right] r \frac{d\psi_m}{dr}\right\}$$

$$- \frac{\psi_m}{(m - nq)^2} \frac{m^2q^2}{r} \left\{\frac{2R_0p'q}{B_0^2}\left[\frac{R_0p'q}{B_0^2} + r\left(\frac{1}{q}\right)'\Delta' + \frac{r}{R_0q}\left(\frac{1}{q^2} - 1\right)\right]\right\}$$

$$+ \frac{\psi_m}{(m - nq)} \frac{mq}{dr} \frac{d}{dr}\left\{2\Delta'\frac{R_0p'q}{B_0^2} - \frac{2}{q}\left[\frac{r}{R_0}\Delta' - \Delta'^2 + \left(\frac{3}{2} - \frac{n^2}{m^2}\right)\frac{r^2}{R_0^2} + \frac{\Delta}{R_0}\right]\right.$$

$$\left. - r\left(\frac{1}{q}\right)'\left[\frac{\Delta}{R_0} - \frac{3}{2}\Delta'^2 + \left(\frac{3}{4} - \frac{n^2}{m^2}\right)\frac{r^2}{R_0^2}\right]\right\}$$

$$- \frac{\psi_m}{(m - nq)} \frac{1}{r} \frac{R_0p'q}{B_0^2}\left[(m + nq)\left(\frac{R_0p'q}{B_0^2} + \frac{r^2}{R_0}\frac{1}{q}\left(\frac{}{}\right)'\right) + 2n(R_0g'q^2)\right]$$

$$- \frac{\psi_m}{(m - nq)} \frac{(m + nq)}{r} (rg')rq\left(\frac{1}{q}\right)'$$

$$- \psi_m \frac{m^2}{r}\left[2\Delta'^2 + \frac{1}{2} r\Delta''(r\Delta'' + 2\Delta') + \frac{r}{R_0}(4\Delta' + r\Delta'') + \frac{\Delta}{R_0} + \frac{9}{4}\frac{r^2}{R_0^2}\right]$$

$$+ \frac{\psi_m}{r}\left[R_0g'q\right]^2 - \psi_m \frac{d}{dr}(rg') \qquad \text{(A.20)}$$

Clearly $L_{m0} \sim 0(1)$, $L_{m2} \sim 0(\varepsilon^2)$, $K_m^{m+1} \sim 0(\varepsilon)$ and $K_m^{m-1} \sim 0(\varepsilon)$. Eqs.(A.16) to (A.20) provide the equations discussed in Sections III-V. As a check on the complicated algebra we have also derived Eqs.(A.16) to (A.20) from a minimization of the energy integral δW for these modes.

Appendix B

General Theory of Δ' in a Torus

In this appendix we develop the general theory of Δ' in a torus and show that the simplified cases treated in the text illustrate the essential generic properties of the problem. This theory encompasses all modes for which the perturbation can be described by the marginal ideal mhd equations at all points in the plasma except in the vicinity of the rational surfaces. Boundary layers at the rational surfaces are assumed to permit discontinuities in the small and large solutions of the ideal equations. The matching of the ideal solutions across the boundary layer determines a relationship that these discontinuities must satisfy. This relationship (like matching to Δ' in a cylinder) contains all the external information needed to determine linear stability; stability can then be discussed for a variety of layer models without recalculating the external solutions. The structure of this relationship between the discontinuities and how it can, in principle, be calculated, is the subject of this appendix.

The marginal ideal mhd equations, obtained from the linearization of $\nabla P = \underset{\sim}{J} \times \underset{\sim}{B}$, are given in Eqs.(A.5) and (A.6) of Appendix A. The poloidal variations are represented there by a Fourier series which is truncated at N poloidal harmonics, the accuracy increasing with N. These poloidal harmonics obey the first order equations, Eqs.(A.8) and (A.9).

First we consider the behaviour of the solutions to Eqs.(A.5) and (A.6) near a rational surface r_s where $m'/n = q(r_s)$. Ordering $r - r_s = x \sim 0(\delta)$ with $\delta \ll 1$, so that $\partial y/\partial r$ and $\partial z/\partial r \sim 0(\delta^{-1})$, Eqs.(A.5) and (A.6) are expanded in δ to obtain

$$y = (C_L \mathrm{sign} x |x|^{p-} + C_S |x|^{p+}) e^{im'\theta} + \bar{y}(\theta) + 0(\delta) \qquad (B.1)$$

and similarly for z. $\bar{y}(\theta)$ is a solution which is finite and continuous through the rational surface, but discontinuities are allowed in C_L and C_S, the coefficients of the large and small solutions. The Mercier indices p_+ and p_- are,[12]

$$p_\pm = -\frac{1}{2} \pm \sqrt{-D_M} \qquad (B.2)$$

where

$$D_M = -\frac{1}{4} + \frac{q}{q'}\frac{p'}{B_0{}^2 f^2} < \frac{R^2}{R_0{}^2}\frac{1}{|\nabla r|^2} > - \frac{q^2}{q'^2}\left(\frac{p'}{B_0{}^2 f^2}\right)^2 < \frac{R^2}{R_0{}^2}\frac{1}{|\nabla r|^2} >^2$$

$$- \left(\frac{p'}{B_0{}^2 f^2}\right)\frac{1}{q'^2}\left(\frac{r}{R_0}\right)^2 \frac{1}{f^2} < \frac{\partial}{\partial r}\left(\frac{R^2}{R_0{}^2}\right) - \frac{R^2}{R_0{}^2}\frac{r}{f}\frac{\partial}{\partial r}\left(\frac{f}{r}\right) > < \frac{R^2 B^2}{B_0{}^2 R_0{}^2 |\nabla r|^2} >$$

$$+ \left(\frac{p'}{B_0{}^2 f^2}\right)^2 \frac{1}{q'^2}\left(\frac{r}{R_0}\right)^2 < \frac{R^4}{R_0{}^4 |\nabla r|^2} > < \frac{B^2}{B_0{}^2}\frac{R^2}{R_0{}^2}\frac{1}{|\nabla r|^2} > \qquad (B.3)$$

with

$$< A > = \frac{1}{2\pi}\int_0^{2\pi} d\theta\, A \,. \qquad (B.4)$$

The behaviour near the rational surface differs in some respects from the cylinder. The resonant poloidal harmonic (i.e. the m' harmonic) has contributions from the small, large and the continuous solutions. The

contribution to the resonant harmonic from the continuous solution is present because of toroidal coupling to non-resonant poloidal harmonics and is therefore a purely toroidal effect. The presence of the continuous solutions means that the solutions of Eqs. (A.5) and (A.6) on either side of a rational surface are not independent.

It is convenient to represent the discontinuities at the rational surface in terms of their odd and even parts since layer equations are usually parity conserving and therefore separate naturally in this way. Let

$$\lim_{|x|\to 0} y_{odd}(x) = \left\{|x|^{p}_{-} + \frac{\Delta'}{2}\,|x|^{p}_{+}\right\} \text{sign } x \qquad \text{(B.5)}$$

and

$$\lim_{|x|\to 0} y_{even}(x) = \left\{\frac{\Gamma'}{2}\,|x|^{p}_{-} + |x|^{p}_{+}\right\} \qquad \text{(B.6)}$$

A series of basic solutions is defined in essentially the same way as in Section II. We consider a problem with rational surfaces at r_m and r_{m+1} where $q(r_m) = m/n$ and $q(r_{m+1}) = (m+1)/n$. The basic solutions are represented as N dimensional vectors $\underset{\sim}{y}(r)$, where $y_k(r)$ is the k^{th} poloidal harmonic. We define the first N basis solutions $\underset{\sim}{y}^{i}(r)$ $(1 \leqslant i \leqslant N)$ to be independant and regular at $r=0$ and to have no discontinuities in large, small or continuous solutions at the rational surfaces. Four more basis solutions are defined thus: $\underset{\sim}{y}^{N+1} = \underset{\sim}{y}^{mS}(r)$ is zero for r less than r_m and propagates from r_m as the small solution only (i.e. no large or continuous solution); $\underset{\sim}{y}^{N+2} = \underset{\sim}{y}^{mL}(r)$ is zero for

r less than r_m and propagates from r_m with the large solution only. $\chi^{N+3} = \chi^{m+1S}(r)$ and $\chi^{N+4} = \chi^{m+1L}(r)$ are similarly defined for the $(m+1)^{th}$ rational surface.

When $0 < r < r_m$ we represent the solution as a linear combination of the N basis solutions χ^i

$$\chi(r) = \sum_{i=0}^{N} \alpha_i \chi^i(r) . \tag{B.7}$$

In the region $r_m < r < r_{m+1}$ the solution is

$$\chi(r) = \sum_{i=0}^{N} \alpha_i \chi^i(r) + \alpha_{mL} \chi^{mL}(r) + \alpha_{mS} \chi^{mS}(r) \tag{B.8}$$

We define C_{mL} to be the amount of large solution and C_{mS} the amount of small as $r \to r_m - 0$. If C^i_{mL} is the amount of large and C^i_{mS} the amount of small solution in $\chi^i(r)$ at r_m, then

$$C_{mL} = \sum_{i=0}^{N} \alpha_i C^i_{mL} \qquad C_{mS} = \sum_{i=0}^{N} \alpha_i C^i_{mS} , \tag{B.9}$$

In the neighbourhood of the rational surface the large and small solutions in Eqs.(B.7) and (B.8) can be written as linear combinations of the odd and even solutions of Eqs.(B.5) and (B.6). Comparing these two representations yields α_{mL} and α_{mS} in terms of C_{mL}, C_{mS}, Δ_m' and

Γ_m'

$$\left[2\underset{\approx}{I} - \begin{bmatrix} \Delta_m' & 0 \\ 0 & \Gamma_m' \end{bmatrix} \begin{bmatrix} 0 & 1 \\ 1 & 0 \end{bmatrix} \right] \begin{bmatrix} \alpha_{mS} \\ \alpha_{mL} \end{bmatrix} = 2 \begin{bmatrix} \Delta_m' & 0 \\ 0 & \Gamma_m' \end{bmatrix} \begin{bmatrix} C_{mL} \\ C_{mS} \end{bmatrix} \quad (B.10)$$

where $\underset{\approx}{I}$ is the unit matrix. The solution for $r_{m+1} < r \leq a$, where a is the radius of the wall, is

$$\underset{\sim}{\chi}(r) = \sum_{i=0}^{\infty} \alpha_i \underset{\sim}{\chi}^i(r) + \alpha_{mL} \underset{\sim}{\chi}^{mL}(r) + \alpha_{mS} \underset{\sim}{\chi}^{mS}(r)$$

$$+ \alpha_{m+1L} \underset{\sim}{\chi}^{m+1L}(r) + \alpha_{m+1S} \underset{\sim}{\chi}^{m+1S}(r) \quad (B.11)$$

Proceeding at r_{m+1} in the same manner we find

$$\left[2\underset{\approx}{I} - \begin{bmatrix} \Delta_{m+1}' & 0 \\ 0 & \Gamma_{m+1}' \end{bmatrix} \begin{bmatrix} 0 & 1 \\ 1 & 0 \end{bmatrix} \right] \begin{bmatrix} \alpha_{m+1S} \\ \alpha_{m+1L} \end{bmatrix} = 2 \begin{bmatrix} \Delta_{m+1}' & 0 \\ 0 & \Gamma_{m+1}' \end{bmatrix} \begin{bmatrix} C_{m+1L} \\ C_{m+1S} \end{bmatrix} \quad (B.12)$$

and

$$C_{m+1L} = \sum_i \alpha_i C_{m+1L}^i + \alpha_{mL} C_{m+1L}^{mL} + \alpha_{mS} C_{m+1L}^{mS}$$

$$C_{m+1S} \quad \sum_i \alpha_i C_{m+1S}^i + \alpha_{mL} C_{m+1S}^{mL} + \alpha_{mS} C_{m+1S}^{mS} \quad (B.13)$$

where C_{m+1L}^i is the amount of large solution in the i^{th} basis solution at r_{m+1} and C_{m+1L}^{mL} is the amount of large solution in $\underset{\sim}{\chi}^{mL}(r)$ at r_{m+1}. At the wall we impose the physical boundary condition $\underset{\sim}{\chi} = 0$ which

can be written in the matrix form

$$\underset{\approx}{A} \cdot \underset{\sim}{\alpha} = - \underset{\approx}{B} \cdot \underset{\sim}{\alpha}' \tag{B.14}$$

where $\underset{\sim}{\alpha}$ is the vector with components $\alpha_i (1 \leqslant i \leqslant N)$, $\underset{\approx}{A}$ is the square matrix

$$A_{ij} = y_i^j(a) \tag{B.15}$$

$\underset{\approx}{B}$ is a matrix with 4 columns and N rows

$$\underset{\approx}{B} = \left(\underset{\sim}{y}^{mS}(a), \underset{\sim}{y}^{mL}(a), \underset{\sim}{y}^{m+1S}(a), \underset{\sim}{y}^{m+1L}(a) \right) \tag{B.16}$$

and

$$\underset{\sim}{\alpha}' = \begin{bmatrix} \alpha_{mS} \\ \alpha_{mL} \\ \alpha_{m+1S} \\ \alpha_{m+1L} \end{bmatrix} \tag{B.17}$$

Defining

$$\underset{\approx}{\Delta}' = \begin{bmatrix} \Delta'_m & 0 & 0 & 0 \\ 0 & \Gamma'_m & 0 & 0 \\ 0 & 0 & \Delta'_{m+1} & 0 \\ 0 & 0 & 0 & \Gamma'_{m+1} \end{bmatrix} \tag{B.18}$$

Eqs.(B.9) and (B.13) can be cast in matrix form

$$\begin{bmatrix} C_{mL} \\ C_{mS} \\ C_{m+1L} \\ C_{m+1S} \end{bmatrix} = \underset{\approx}{C} \cdot \underset{\sim}{\alpha} + \underset{\approx}{D} \cdot \underset{\sim}{\alpha}' \qquad (B.19)$$

where $C_{1i} = C^{i}_{mL}$, $C_{2i} = C^{i}_{mS}$, $C_{3i} = C^{i}_{m+1L}$, $C_{4i} = C^{i}_{m+1S}$ and the non-vanishing components of $\underset{\approx}{D}$ are $D_{31} = C^{mS}_{m+1L}$, $D_{32} = C^{mL}_{m+1L}$, $D_{41} = C^{mS}_{m+1S}$ and $D_{42} = C^{mL}_{m+1S}$. From Eqs.(B.10), (B.12), (B.14) and (B.19) we obtain

$$\left(\underset{\approx}{I} + \underset{\approx}{\Delta}' \cdot \underset{\approx}{E}\right) \cdot \underset{\sim}{\alpha}' = 0 \qquad (B.20)$$

with

$$\underset{\approx}{E} = - \underset{\approx}{F} + \underset{\approx}{C} \cdot \underset{\approx}{A}^{-1} \cdot \underset{\approx}{B} - \underset{\approx}{D} \qquad (B.21)$$

where $\underset{\approx}{F}$ has non-vanishing elements $F_{12} = F_{21} = F_{34} = F_{43} = 1/2$. Thus the layer quantities satisfy the equation

$$\left|\underset{\approx}{I} + \underset{\approx}{\Delta}' \cdot \underset{\approx}{E}\right| = 0 \qquad (B.22)$$

Eq.(B.21) summarises all the external ideal mhd information needed to calculate the growth rate from a variety of layer models. The layer physics yields $\Delta'_m = \Delta_m(\omega)$, $\Delta'_{m+1} = \Delta_{m+1}(\omega)$, $\Gamma'_m = \Gamma_m(\omega)$ and $\Gamma'_{m+1} = \Gamma_{m+1}(\omega)$; substituting these expressions into Eq.(B.22) completes

the dispersion relation.

For the frequency range of interest it is often possible to set $\Gamma' = 0$. In order to see this we consider a layer in which the characteristic scale length and frequency are δ and ω_0 and we define scaled variables $X = x/\delta$ and $Q = \omega/\omega_0$. In these variables the layer equations have no large or small parameters and we obtain odd and even solutions with asymptotic behaviour

$$y_{\substack{odd \\ |X| \to \infty}}(X) = \{|X|^{p_-} + \frac{\Delta_+(Q)}{2} |X|^{p_+}\} \text{ sign } X \tag{B.23}$$

$$y_{\substack{even \\ |X| \to \infty}}(X) = \{\frac{\Delta_-(Q)}{2} |X|^{p_-} + |x|^{p_+}\} \tag{B.24}$$

in the notation of Ref. 25. Matching to Eqs.(B.5) and (B.6) yields

$$\Delta' = \frac{\Delta_+(Q)}{\delta^{(p_+ - p_-)}}$$

$$\Gamma' = \Delta_-(Q)\, \delta^{(p_+ - p_-)} \tag{B.25}$$

where $p_+ - p_- > 0$. Since we expect that $Q \sim 0(1)$ and $\Delta_+ \sim \Delta_- \sim 0(1)$, we see that Δ' is large and Γ' small. In fact, in resistive mhd[25] $Q << 1$ for $\Delta' \sim 0(1)$ and Δ_- is usually small, implying that Γ' is doubly small. Although one should examine the particular layer theory involved to determine whether Γ' is indeed small, we will assume the

behaviour above. Of course, close to ideal instability boundary $\Delta' \to \infty$ and Γ' can become important, but, as this limit is experimentally indistinguishable from the ideal mode, we do not consider it. Eqs.(B.10) and (B.12) with $\Gamma' = 0$ yield $\alpha_{mL} = 0$ and $\alpha_{m+1L} = 0$ and the dispersion relation reduces to

$$\left| \underset{\approx}{I} + \underset{\approx}{\Delta}' \cdot \underset{\approx}{E} \right| = 0, \qquad \text{(B.26)}$$

with $\underset{\approx}{E}$ a 2×2 matrix and $\underset{\approx}{\Delta}'$ given by Eq.(20). Eq.(B.26) is precisely the same as Eq.(24) of Section II, so that the hyperbolic structure, Eq.(25), is generic to the two rational surface problem. Thus the simplified problem treated in Section II, where only three poloidal harmonics are considered, reproduces the correct form of the relation between the Δ''s, Eq.(24), although the matrix $\underset{\approx}{E}$ is only approximate.

The generalisation to M rational surfaces is straight forward. The first N basis solutions are defined as before and at each of the M rational surfaces two basis solutions are launched, one of which is purely a small solution $\chi^{jS}(r)$ and the other is purely a large solution $\chi^{jL}(r)$. While the matrices $\underset{\approx}{A}$ and $\underset{\approx}{C}$ retain their earlier definitions, $\underset{\approx}{B}$ is redefined as a 2M column, N row matrix with the $2j-1^{th}$ column being $\chi^{jS}(a)$ and the $2j^{th}$ being $\chi^{jL}(a)$. The vector $\underset{\sim}{\alpha}'$ is such that $\alpha_{2j-1} = \alpha_{jS}$ and $\alpha_{2j} = \alpha_{jL}$ where α_{jS} and α_{jL} are the factors multiplying χ^{jS} and χ^{jL} in the eigenvector. The elements of $\underset{\approx}{D}$ are given by $D_{2j-1,2i-1} = C^{iS}_{jL}$, $D_{2j-1,2i} = C^{iL}_{jL}$, $D_{2j,2i-1} = C^{iS}_{jS}$ and

$D_{2j,2i} = C_{jS}^{iL}$, where, for example, C_{jS}^{iL} is the amount of small solution at the j^{th} surface in the basis solution $\underset{\sim}{y}^{jL}(r)$ which was launched at the i^{th} surface as a large solution. Similar definitions hold for the other quantities, implying $C_{jS}^{iS} = C_{jL}^{iL} = C_{jS}^{iL} = C_{jL}^{iS} = 0$ if $i \geq j$. $\underset{\approx}{F}$ and $\underset{\approx}{\Delta}'$ are 2M by 2M matrices where

$$F_{2j-1,2j} = F_{2j,2j-1} = \frac{1}{2}$$

$$F_{ij} = 0 \quad \text{otherwise} \tag{B.27}$$

$$\Delta'_{i,2j-1} = \delta_{i,2j-1}\ \Delta'_j$$

$$\Delta'_{i,2j} = \delta_{i,2j}\ \Gamma'_j \tag{B.28}$$

With these definitions we recover the expression

$$\left(\underset{\approx}{I} + \underset{\approx}{\Delta}' \cdot \underset{\approx}{E}\right) \cdot \underset{\sim}{\alpha}' = 0, \tag{B.29}$$

where $\underset{\approx}{E} = -\underset{\approx}{F} + \underset{\approx}{C}.\underset{\approx}{A}^{-1}.\underset{\approx}{B} - \underset{\approx}{D}$. The determinantal equation $\left|\underset{\approx}{I} + \underset{\approx}{\Delta}' \cdot \underset{\approx}{E}\right| = 0$ now defines a hyperboloid in the 2M dimensional Δ'_j, Γ'_j space. Again setting $\Gamma'_j = 0$ reduces Eq.(B.29) to a hyperboloid of M dimensions.

The definition of Δ' given in Eq.(B.5) is not the familiar definition of Ref. 3 where Δ' is the jump in the ratio of large to small solutions across the rational surface, although the two definitions

coincide when Γ' is zero. However our definitions, Eqs.(B.5) and (B.6), simplify matching to parity conserving layer equations. Finally it is interesting to note that the regions separated by a rational surface are not physically independant in a torus since they are connected by the continuous solution, whereas in a cylinder they are disjoint.

References

1. J.A. Wesson, Nuclear Fusion 16 130 (1966)
2. H.P. Furth, J. Killeen and M.N. Rosenbluth, Phys. Fluids 6 459 (1963).
3. B. Coppi, J.M. Greene and J.L. Johnson, Nucl. Fusion 6 101 (1966).
4. H.P. Furth, P.H. Rutherford and H. Selberg, Phys. Fluids 16 1054 (1973).
5. B. Coppi, Phys. Fluids 7 1501 (1964).
6. J.F. Drake and Y.C. Lee, Phys. Fluids 20 1341 (1977).
7. S.C. Cowley, R.M. Kulsrud and T.S. Hahm, Phys. Fluids 29 3230 (1986).
8. J.A. Holmes, B.A. Carreras, H.R. Hicks, V.E. Lynch and K.E. Rothe, Phys. Fluids 25 800 (1982).
9. R. Izzo, D.A. Monticello, J. De Lucia, W. Park and C.M. Ryu, Phys. Fluids 28 903 (1985).
10. L.A. Charlton, J.A. Holmes, H.R. Hicks, V.E. Lynch and B.A. Carreras, J. Comp. Phys. 63 107 (1986).
11. T.C. Hender, R.J. Hastie and D.C. Robinson, to be published in Nucl. Fusion.
12. A.H. Glasser, J.M. Greene and J.L. Johnson, Phys. Fluids 18 875 (1975).
13. J.C. Callen, W.X. Qu, K.D. Siebert, B.A. Carreras. K.C. Shaing and D.A. Spong, to be published in Plasma Physics and Controlled Nuclear Fusion Research (Proc. 11th Int. Conf. Kyoto, 1986) IAEA Vienna.

14. R.C. Grimm, R.L. Dewar, J. Manickam, S.C. Jardin, A.H. Glasser and M.S. Chance, in Plasma Physics and Controlled Nuclear Fusion Research (Proc. 9th Int. Conf., Baltimore 1982) Vol.3, IAEA Vienna (1983) 35.

15. M.N. Bussac, D. Edery, R. Pellat and J.L. Soule, in Plasma Physics and Controlled Nuclear Fusion Research (Proc. 6th Int. Conf., Berchtesgaden 1976) Vol.1 IAEA Vienna (1977) 607.

16. D. Edery, J.L. Soule, R. Pellat, M. Fray and J.P. Somon, in Plasma Physics and Controlled Nuclear Fusion Research (Proc. 8th Int. Conf., Brussels, 1980) Vol.1, IAEA Vienna (1981) 269.

17. B.A. Carreras, H.R. Hicks and D.K. Lee, Phys. Fluids 24 66 (1981).

18. W.A. Newcomb, Ann. Phys. (NY) 10 232 (1960).

19. P.H. Rutherford, Phys. Fluids 16 1903 (1973).

20. M. Kotschenreuther, R.D. Hazeltine and P.J. Morrison, Phys. Fluids 28 294 (1985).

21. B. Coppi, R. Galvao, R. Pellat, M.N. Rosenbluth and P.H. Rutherford, Sov. J. Plasma Phys. 2 533 (1976) [Fiz Plazmy 2 961 (1976)].

22. J.W. Connor and R.J. Hastie, Culham Report CLM-M106 (1985).

23. M.N. Bussac, R. Pellat, D. Edery and J.L. Soule, Phys. Rev. Letts. 35 1638 (1975).

24. A.B. Mikhailovskii, Nuclear Fusion 14 483 (1974).

25. A.H. Glasser, S.C. Jardin and G. Tesauro, Phys. Fluids 27 1225 (1984).

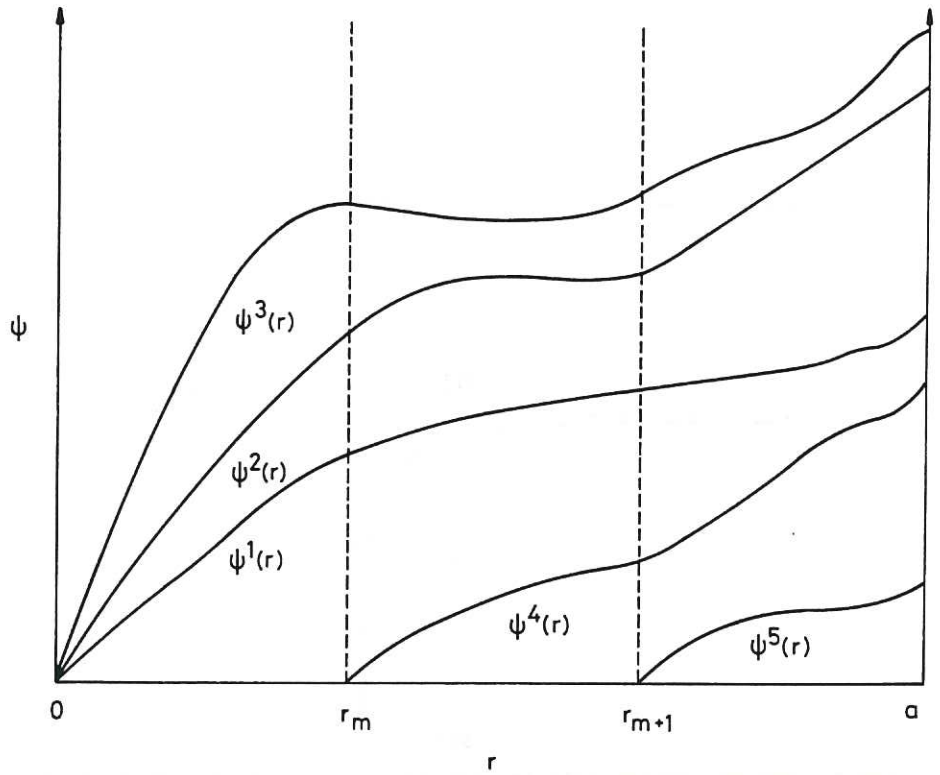

Fig.1 The radial structure of the main components of the five basis solutions for the case of three poloidal harmonics and two rational surfaces.

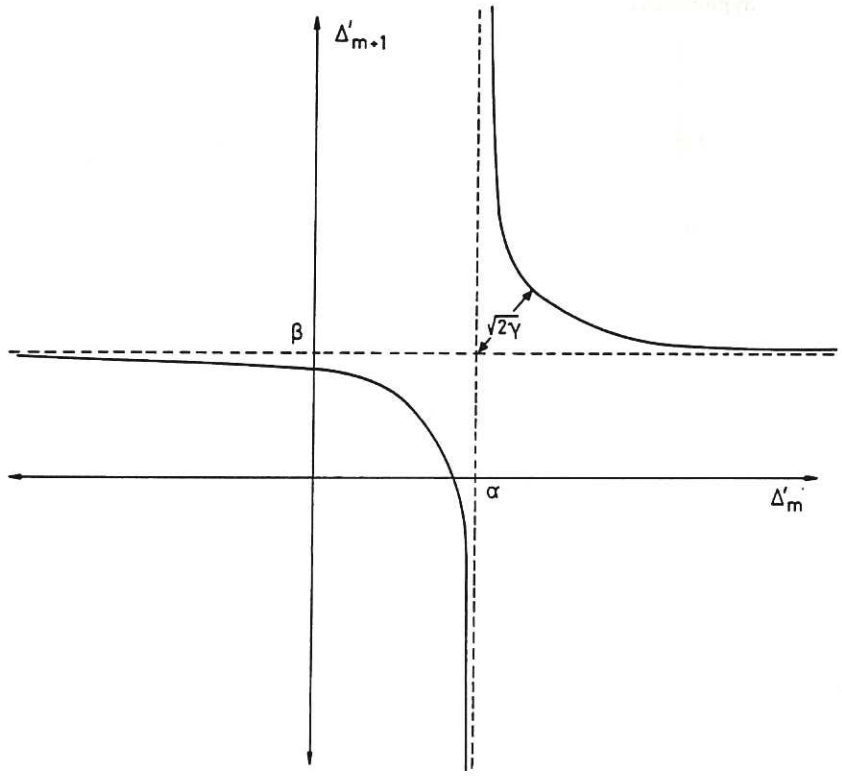

Fig.2 The hyperbolic relation between Δ'_{m+1} and Δ'_m showing the asymptotes $\Delta'_m = \alpha$ and $\Delta'_{m+1} = \beta$ and the coupling parameter γ.

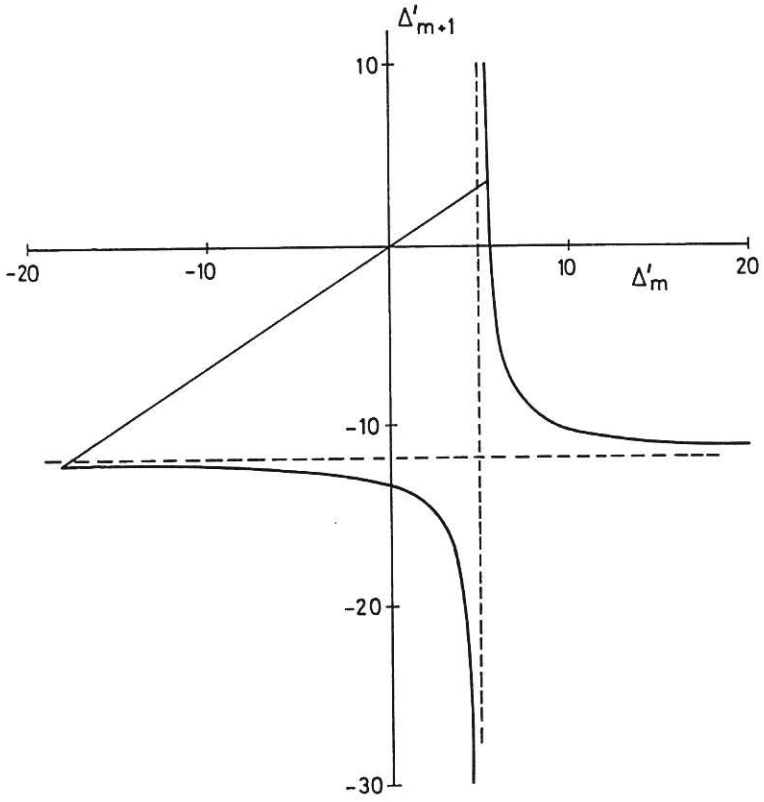

Fig.3 The hyperbolic relation between Δ'_{m+1} and Δ'_m when the toroidal coupling is due to finite pressure in a large aspect ratio torus with $\beta R/a = 0.08$. Growth rates for the layer model of Eq.(3) are given by an intersection of a line through the origin with the hyperbola.

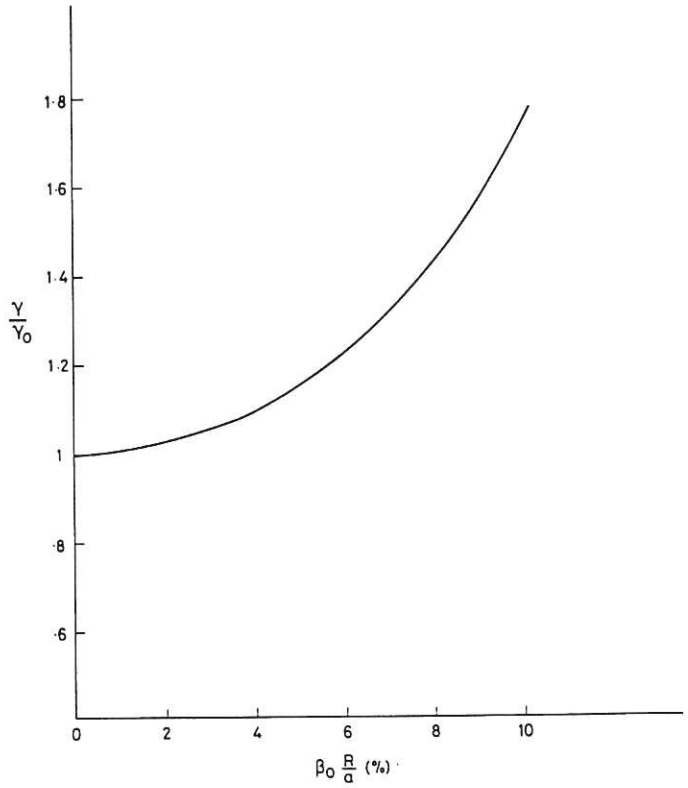

Fig.4 The variation of normalised growth rate γ/γ_0 with $\beta R/a$ where γ_0 is the growth rate in a cylinder.

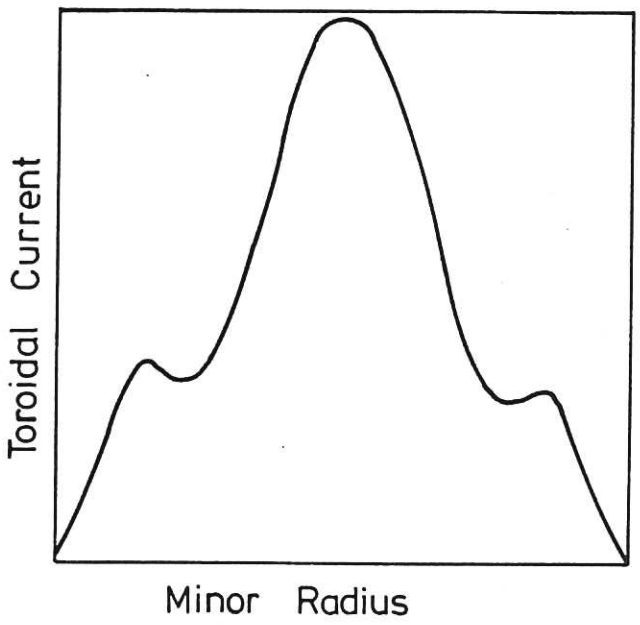

Fig.5 A current profile for an equilibrium with $\beta = 0$, $R/a = 10$ and $1.3 < q < 3.6$.

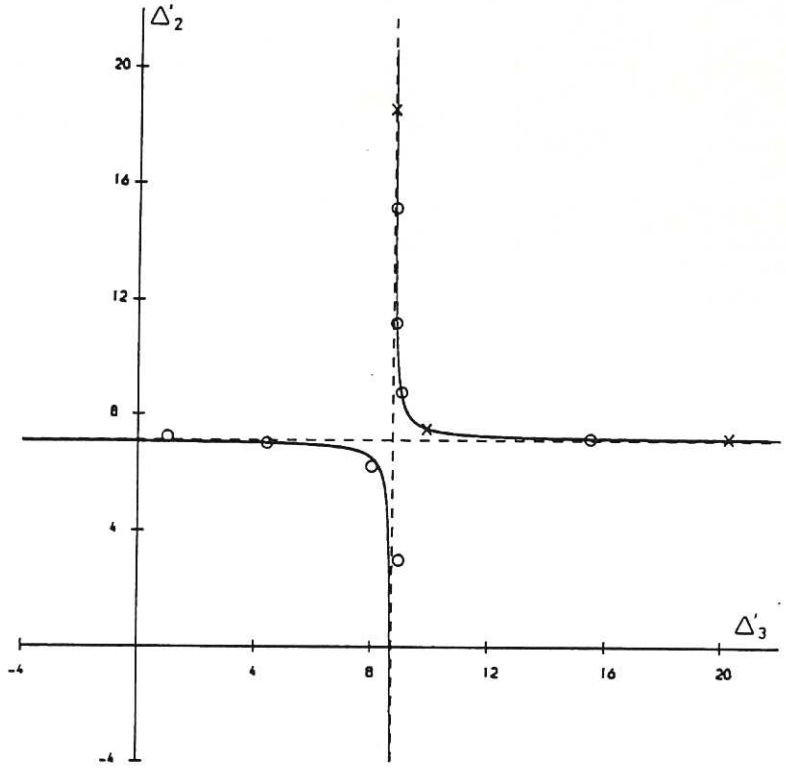

Fig.6 The hyperbolic relation between Δ'_{m+1} and Δ'_m for the equilibrium of Fig.5 calculated using the FAR code. Crosses are the points used to construct the hyperbola and circles are checks on the validity of the method.